

MedFrameQA: A Multi-Image Medical VQA Benchmark for Clinical Reasoning

Suhao Yu^{1*} Haojin Wang^{2*} Juncheng Wu^{3*} Luyang Luo⁴ Jingshen Wang⁵
Cihang Xie³ Pranav Rajpurkar⁴ Carl Yang⁶ Yang Yang⁷ Kang Wang⁷ Yannan Yu⁷
Yuyin Zhou³

¹University of Pennsylvania ²University of Illinois Urbana-Champaign ³UC Santa Cruz
⁴Harvard University ⁵UC Berkeley ⁶Emory University ⁷UC San Francisco

Abstract

Real-world clinical practice demands multi-image comparative reasoning, yet current medical benchmarks remain limited to single-frame interpretation. We present MEDFRAMEQA, the first benchmark explicitly designed to test multi-image medical VQA through educationally-validated diagnostic sequences. To construct this dataset, we develop a scalable pipeline that leverages narrative transcripts from medical education videos to align visual frames with textual concepts, automatically producing 2,851 high-quality multi-image VQA pairs with explicit, transcript-grounded reasoning chains. Our evaluation of 11 advanced MLLMs (including reasoning models) exposes severe deficiencies in multi-image synthesis, where accuracies mostly fall below 50% and exhibit instability across varying image counts. Error analysis demonstrates that models often treat images as isolated instances, failing to track pathological progression or cross-reference anatomical shifts. MEDFRAMEQA provides a rigorous standard for evaluating the next generation of MLLMs in handling complex, temporally grounded medical narratives.

1 Introduction

Multimodal Large Language Models (MLLMs) have quickly emerged as a powerful paradigm for enabling advanced AI systems in clinical and medical domains (Xie et al., 2025; OpenAI, 2023a; Li et al., 2023; Tu et al., 2023; Saab et al., 2024; Huang et al., 2025; Wu et al., 2025). In practice, clinicians frequently employ multi-image diagnostic workflows, comparing related scans and synthesizing findings across different views and time points. Current evaluation benchmarks, however, focus predominantly on isolated, single-image analysis, *e.g.*, (Lau et al., 2018; Ben Abacha et al., 2019, 2021; He et al., 2020; Liu et al., 2021; Zhang et al., 2023; Hu et al., 2024; Chen et al., 2024). The left

panel of Figure 1 shows a typical SLAKE (Liu et al., 2021) example whose answer requires nothing more than basic object recognition in one frame. In everyday care, however, clinicians rarely rely on a lone snapshot; they routinely compare multiple images taken from different views, modalities, or time points before making a diagnosis.

Only recently has the multimodal reasoning literature begun to systematically study multi-image VQA. A small number of recent benchmarks, such as Yue et al. (2024a,b); Zuo et al. (2025), introduce questions that explicitly reference multiple images. Yet these tasks still fall short of the integrative reasoning required in medicine, as images are often treated as independent clues rather than complementary views of a coherent clinical scenario. As illustrated by the MedXpertQA (Zuo et al., 2025) example in the middle panel of Figure 1, the two images lack a clear physiological or causal connection, allowing models to answer correctly without truly synthesizing information across images. As a result, performance on such datasets provides limited evidence of a system’s ability to perform clinically grounded cross-image reasoning.

To bridge this gap, we introduce MEDFRAMEQA, the first benchmark explicitly designed to test multi-image reasoning in medical VQA by leveraging YouTube’s rich repository of medical education videos (Osman et al., 2022; Akakpo and Akakpo, 2024). Our approach focuses on educational video sequences with temporally and semantically connected visual content that demonstrate diagnostic reasoning within coherent clinical presentations. Building on this insight and inspired by prior work (Ikezogwo et al., 2023), we propose a scalable VQA generation pipeline that automatically constructs multi-image VQA questions from keyframes extracted from 3,420 medical videos, covering 9 human body systems and 43 organs. We curate medical education videos via combinatorial search, extract and filter keyframes, tran-

*Equal contribution.

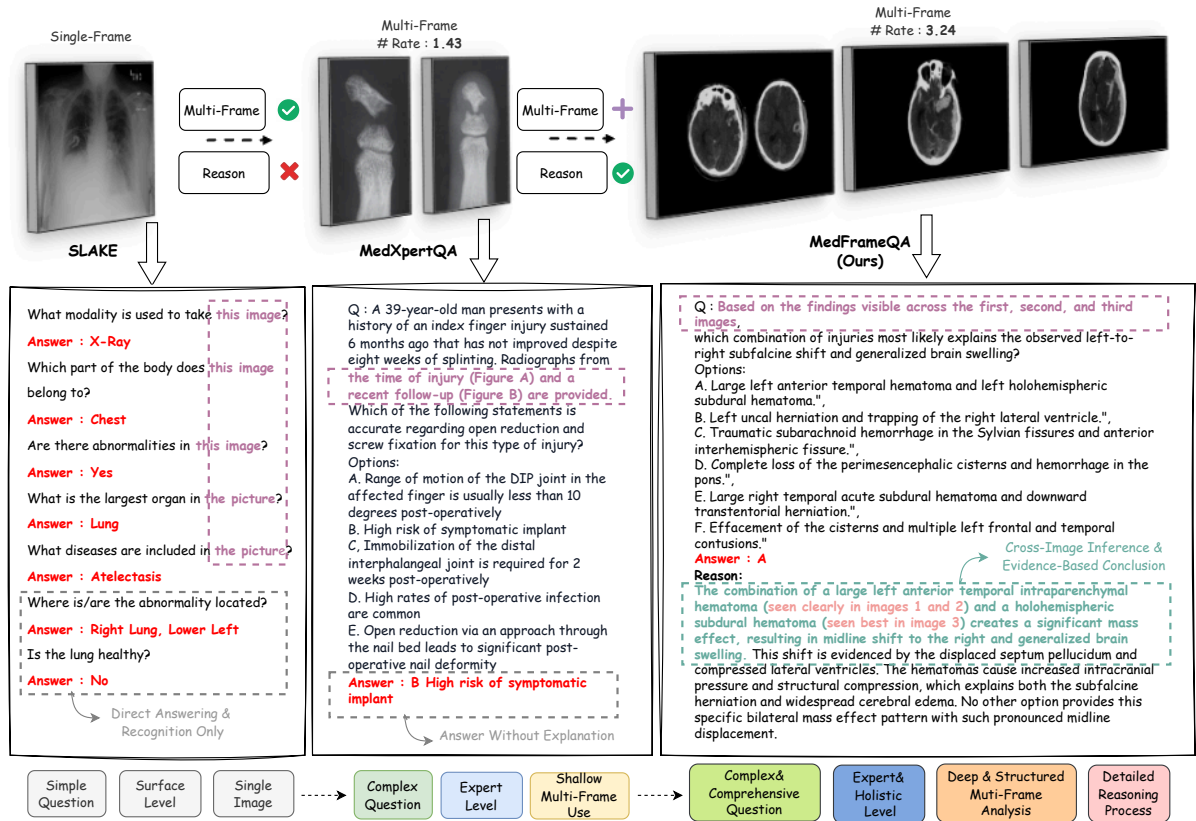


Figure 1: **Comparison of medical VQA benchmarks.** MEDFRAMEQA introduces multi-image, clinically grounded questions that require comprehensive reasoning across all images. Unlike prior benchmarks such as SLAKE (Liu et al., 2021) and MedXpertQA (Zuo et al., 2025), it emphasizes diagnostic complexity, expert-level knowledge, and explicit reasoning chains. **Rate** in the figure means the average number of images per question.

scribe and temporally align narrations, and merge clinically related frame-text pairs into coherent multi-frame clips. Finally, we generate multiple-choice VQA items requiring cross-image clinical reasoning and apply two-stage automated and manual filtering to ensure benchmark quality.

This pipeline yields MEDFRAMEQA, consisting of 2,851 challenging multi-image VQA questions that require reasoning over temporally coherent sequences of 2–5 frames. Each instance pairs a natural-language query with multiple related frames—such as multi-view anatomy, disease progression within educational narratives, or cross-modal comparisons—drawn from continuous medical videos rather than arbitrary image collections (Figure 1, right). To support grounded reasoning, we provide gold-standard rationales derived from source video transcripts, explicitly linking each frame to the final answer. Beyond the benchmark itself, our work introduces a systematic pipeline for aligning audio narrations with visual frames at scale, offering a new perspective on constructing multimodal reasoning datasets from large video cor-

pora. We benchmark 11 state-of-the-art MLLMs on MEDFRAMEQA and find that their accuracies mostly fall below 50%, with substantial variation across body systems, organs, and modalities, revealing critical gaps between current multimodal model capabilities and the demands of clinically grounded, video-derived multi-image reasoning.

2 Related Work

Reasoning Multimodal Large Language Models Recent interest in MLLM reasoning has extended to medical tasks like diagnostics and clinical decision-making (Wang et al., 2024; Xie et al., 2024; Chen et al., 2025; Deng et al., 2025; Al-Saad et al., 2024; Jiang et al., 2025). While generalist models like Llava-Med (Li et al., 2023) and GPT-4V (OpenAI, 2023b) show promise, they often lack interpretable reasoning. To address this, recent works employ strategies such as multi-expert prompting (MedCoT (Wang et al., 2025)), reinforcement learning for plausible rationales (MedVLM-R1 (Pan et al., 2025)), and long-context modeling (Med-Gemini (Saab et al., 2024), Med-

Benchmark	# Images	# Questions	# Rate	Multi-Image	Real World Scenarios	Paired Reasoning Across Multi Img.
VQA-RAD (Lau et al., 2018)	315	3515	0.09	✗	✗	✗
VQA-Med-2019 (Ben Abacha et al., 2019)	500	500	1.00	✗	✗	✗
VQA-Med-2021 (Ben Abacha et al., 2021)	500	500	1.00	✗	✗	✗
PathVQA (He et al., 2020)	858	6,719	0.13	✗	✗	✗
SLAKE-En (Liu et al., 2021)	96	1,061	0.09	✗	✗	✗
PMC-VQA (Zhang et al., 2023)	29,021	33,430	0.87	✗	✗	✗
OmniMedVQA (Hu et al., 2024)	118,010	127,995	0.92	✗	✗	✗
GMAI-MMBench (Chen et al., 2024)	21,180	21,281	1.00	✗	✗	✗
MMMU (H&M) (Yue et al., 2024a)	1,994	1,752	1.14	✓	✗	✓
MMMU-Pro (H&M) (Yue et al., 2024b)	431	346	1.25	✓	✗	✓
MedXpertQA MM (Zuo et al., 2025)	2852	2000	1.43	✓	✓	✗
MEDFRAMEQA	9237	2851	3.24	✓	✓	✓

Table 1: **Comparison of MEDFRAMEQA with Existing Benchmarks.** MEDFRAMEQA supports multi-image reasoning within real-world clinical video scenarios and paired reasoning across frames. The paired reasoning in MEDFRAMEQA is derived from the transcripts from original video clips.

Gemma3 (Sellergren et al., 2025a)). These advances highlight the need for rigorous benchmarks to evaluate medical reasoning capabilities.

Multimodal Medical Benchmarks Existing benchmarks for evaluating medical MLLMs remain limited in scope, with most focusing on single-image VQA. Early datasets such as VQA-RAD (Lau et al., 2018), VQA-Med-2019 (Ben Abacha et al., 2019), VQA-Med-2021 (Ben Abacha et al., 2021), SLAKE (Liu et al., 2021), and PathVQA (He et al., 2020) primarily target isolated questions within specific medical subdomains. More recent benchmarks, including PMC-VQA (Zhang et al., 2023), OmniMedVQA (Hu et al., 2024), and GMAI-MMBench (Chen et al., 2024), broaden domain coverage but still largely operate in a single-image setting. Although recent efforts such as MMMU (H&M) (Yue et al., 2024a), MMMU-Pro (H&M) (Yue et al., 2024b), and MedXpertQA MM (Zuo et al., 2025) incorporate multi-image VQA, they lack clinically grounded cross-image reasoning and gold-standard rationales, limiting their ability to assess genuine multi-image reasoning. We provide a detailed comparison with existing benchmarks in Section 1.

Video Data For Medical Benchmarking Recent work has explored leveraging video data for medical dataset construction, enabled in part by advances in speech recognition models such as Whisper (Radford et al., 2023). Prior efforts have collected large-scale video–text or image–text datasets from medical videos, including Quilt-1M (Ikezogwo et al., 2023), as well as task-specific benchmarks targeting instructional or procedural content (Gupta et al., 2023; Hu et al., 2023; Ghamsarian et al., 2024). Despite these advances, video data has seen limited use for benchmarking multimodal large language models (MLLMs) in the medical

domain. Notably, medical content on YouTube (Osman et al., 2022; Derakhshan et al., 2019) naturally provides temporally grounded reasoning chains across frames. Motivated by this observation, we leverage YouTube videos and design an automated VQA generation pipeline to construct multi-image questions for evaluating MLLMs under complex, multi-frame clinical scenarios.

3 MedFrameQA Benchmark

3.1 Video Collection

As the first step in building MEDFRAMEQA, we assemble a large pool of clinically relevant videos from YouTube (illustrated in Figure 2(a)). Specifically, we curate 114 carefully designed search queries, each formed by pairing a common imaging modality (*e.g.* MRI, X-Ray, CT, and radiograph) with a frequently encountered disease or finding (*e.g.* brain tumor, pneumonia, chest, and bone fracture). This combinatorial list gives broad coverage of routine diagnostic scenarios; the full set of keywords is provided in Section D. Then, for every query, we retrieve the top related results and discard clips shorter than 5 minutes or longer than 2 hours. The remaining corpus comprises 1,971 high-resolution, narration-rich medical videos that serve as the raw material for MEDFRAMEQA.

3.2 Frame-Caption Pairing

Medical Frame Extraction. To process the raw video collected, the first task is to identify the corresponding medical frames. Following Ikezogwo et al. (2023), we run FFmpeg (<https://ffmpeg.org/>) to extract key-frames—those delineating the scene boundaries and often indicating significant visual transitions—and record the corresponding temporal span of each segment (f_{start}, f_{end}). Each can-

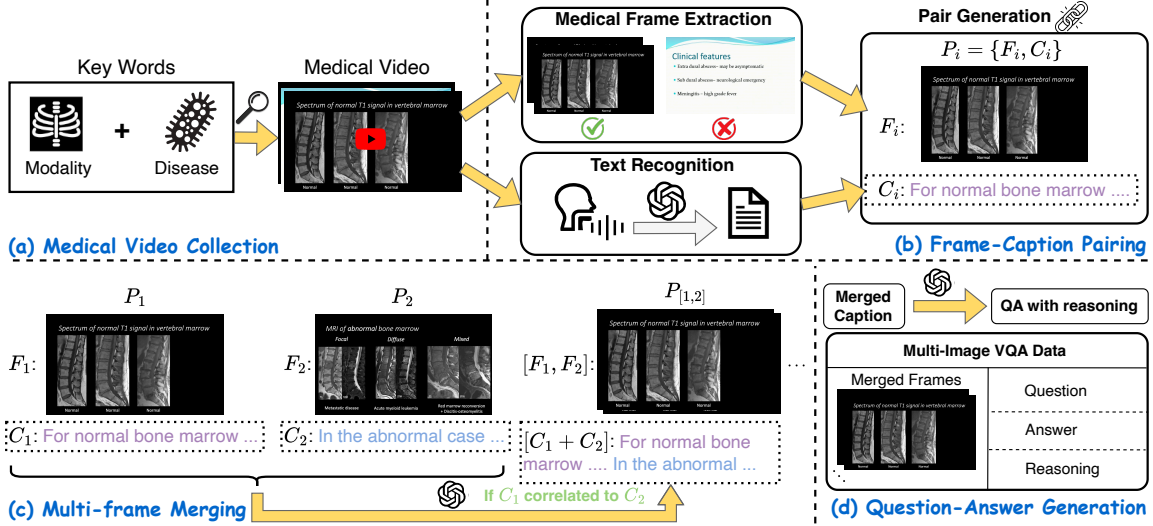


Figure 2: **Data generation pipeline.** (a) Video Collection: Collecting 3,420 medical videos via clinical search queries (Section 3.1). (b) Frame-Caption Pairing: Extracting keyframes and aligning with transcribed captions. (Section 3.2) (c) Multi-Frame Merging: Merging clinically related frame-caption pairs into multi-frame clips. (Section 3.3) (d) Question-Answer Generation: Generating multi-image VQA from the multi-frame clips. (Section 3.4)

didate frame is then evaluated by GPT-4o (Hurst et al., 2024) under four criteria: (1) *image quality*, evaluating the clarity and medical relevance of the frame; (2) *prominence of medical content*, determining if the frame predominantly consists of medical imagery; (3) *informative content*, checking if the frame is understandable and holds significant information; and (4) *privacy*, ensuring the frame excludes unrelated human faces, such as those of presenters in video conferences. Note that only frames satisfying all four requirements are retained. More details about the frame filtering criteria can be found in Section F.

This filtering step leaves us with a sequence of qualified key-frames and their temporal spans:

$$S_F = [F_1, \dots, F_m],$$

$$D_F = [(f_{start}^1, f_{end}^1), \dots, (f_{start}^m, f_{end}^m)],$$
(1)

where m is the number of extracted medical frames. S_F and D_F are the sequence of frames and times.

Text Recognition. We next transcribe the audio track with Whisper (Radford et al., 2023). The model returns a sequence of n text snippets and their time stamps:

$$S_T = [T_1, \dots, T_n],$$

$$D_T = [(t_{start}^1, t_{end}^1), \dots, (t_{start}^n, t_{end}^n)].$$
(2)

Pair Generation. Our third task now is to pair the medical frame with the corresponding caption. Intuitively, each frame can be simply paired with

the text snippets that emerge concurrently with it during the same time interval. However, narration in medical videos can lag behind or precede the exact moment a frame is shown. To associate each frame (F_i) with all relevant speech, we define a symmetric margin (Δ) seconds around the frame’s interval and gather every transcript whose span intersects that window $[f_{start}^i - \Delta, f_{end}^i + \Delta]$. Then all snippets within this window range will be concatenated to form a coarse caption $\tilde{C}_i = [T_j, T_{j+1}, \dots, T_k]$.

Then we leverage GPT-4o to enhance the quality of \tilde{C}_i . Specifically, GPT-4o is instructed to (i) remove statements unrelated to the displayed frame and (ii) refine the description to ensure the correct usage of clinical terminology. Formally,

$$C_i = \text{GPT-4o} \left(\tilde{C}_i, F_i \mid I_{rephrase} \right),$$
(3)

where C_i denotes the refined caption, and $I_{rephrase}$ is the prompt (see Section F for more details). The final frame–caption pair is $P_i = \{F_i, C_i\}$, and the sequence of frame-caption pairs of the entire video is $S_P = [P_1, \dots, P_n]$.

3.3 Multi-Frame Merging

The paired frames described above usually belong to longer narrative units within educational presentations—for example, a radiologist may spend several consecutive slides discussing the same lesion during a structured teaching session. To capture such continuity, we merge adjacent

Model	Accuracy per System									Avg
	CNS	RES	CIR	DIG	URI	REP	END	MSK	AUX	
<i>Proprietary Reasoning Models</i>										
o1	46.91	48.88	49.49	47.45	49.03	42.26	47.68	51.59	48.75	47.91
o3	47.81	52.00	50.00	48.48	50.71	45.02	51.84	54.90	50.41	50.18
o4-mini	46.03	49.78	48.74	48.63	51.85	43.62	52.44	53.38	50.82	49.40
Gemini-2.5-Flash	48.82	58.26	57.21	50.25	48.61	55.81	55.38	60.21	52.85	54.75
Claude-3.7-Sonnet	49.21	46.09	53.23	50.25	49.07	47.57	47.81	52.42	49.59	49.67
<i>Open-Source Reasoning Models</i>										
QvQ-72B-Preview	44.88	46.67	47.43	41.13	45.68	47.00	47.68	49.37	47.15	46.44
<i>Proprietary Non-Reasoning Models</i>										
GPT-4o	48.82	49.13	37.31	50.00	43.98	45.88	46.22	43.60	44.31	45.67
GPT-4o-mini	41.73	36.52	39.30	28.36	35.65	33.83	30.68	34.95	34.96	34.55
GPT-4-Turbo-V	45.28	46.09	42.79	49.75	43.06	48.63	49.80	45.16	46.75	46.69
<i>Open-Source Non-Reasoning Models</i>										
Qwen2.5-VL-72B-Instruct	43.18	47.39	42.29	39.80	39.81	43.41	43.03	44.00	40.11	42.65
<i>Open-Source Non-Reasoning Medical Finetuned Models</i>										
MedGemma-27b-it	49.61	44.20	48.09	43.45	41.36	46.58	50.33	45.62	39.70	45.47

Table 2: **Accuracy of Models on MEDFRAMEQA.** We report the system-wise accuracy of models on MEDFRAMEQA. The results are averaged over all the tasks in MEDFRAMEQA. The best results on each system and average accuracy are highlighted in bold. In general, all assessed models demonstrate persistently low accuracy, with system-wise performance of substantial variability in task difficulty.

frame-caption pairs into multi-frame "clips" whenever their captions describe the same clinical concept within the educational context. The paired caption of each frame already provides a description of its visual content; hence, we rely entirely on the textual correlation between the captions to determine if there is a connection between two frames. Specifically, as illustrated in Figure 2(c), for every consecutive pair $P_i = \{F_i, C_i\}$ and $P_{i+1} = \{F_{i+1}, C_{i+1}\}$, we ask GPT-4o (prompt in Section F) whether these two captions are correlated. If yes, we then combine these two pairs: $P_{[i,i+1]} = \{[F_i, F_{i+1}], [C_i \oplus C_{i+1}]\}$, where \oplus represents the text concatenation. We then compare the merged caption $[C_i \oplus C_{i+1}]$ with the next caption C_{i+2} ; if the relation persists, we append P_{i+2} to the group. This sliding process continues until (i) the next caption is judged unrelated or (ii) the group reaches a maximum of five frames, the limit we adopt in this work.

Applying the above procedure to all videos yields 7,998 multi-frame clips, each containing 2–5 medically coherent frame-caption pairs. These clips constitute the basic building blocks for the subsequent VQA-item generation stage.

3.4 Question Answering Generation

As shown in Figure 2(d), for each merged group $P_{[i,i+1\dots]} = \{[F_i, F_{i+1}, \dots], [C_i \oplus C_{i+1}, \dots]\}$, we instruct GPT-4o to generate challenging multiple-choice questions. Formally,

$$Q, A, R = \text{GPT-4o}([C_i \oplus C_{i+1} \dots] \mid I_{gen}), \quad (4)$$

where Q, A, R are the generated question, the correct answer, and the reasoning, respectively. I_{gen} is the generation prompt, enforcing four requirements: (1) *Information Grounding*: all questions must rely solely on visual evidence explicitly described in the educational video captions; (2) *Educational Clinical Reasoning*: each question should probe skills demonstrated in medical education contexts such as anatomical localization and differential diagnosis within structured presentations; (3) *Contextual Interaction*: the wording must reference the images in order (e.g., "in the first image ..., whereas in the third image ...") and require synthesizing information across the educational sequence; (4) *Distraction Options*: every item includes plausible but incorrect answer choices that differ from the ground truth in clinical details within the educational context. The complete I_{gen} is provided in Section F. Lastly, each clip is packaged as $\{Q, A, R, [F_i, F_{i+1} \dots]\}$, forming a single entry.

Model	Accuracy (%) by Frame Count					Accuracy (%) by Modality				
	2	3	4	5	<i>SD</i>	CT	MRI	Ultrasound	X-ray	Other
o1	48.16	45.64	51.43	48.15	2.37	48.98	45.40	49.05	49.16	51.64
o3	50.00	47.46	53.60	51.38	2.57	50.09	48.57	51.45	53.06	52.38
o4-mini	50.21	46.23	50.00	50.37	1.99	48.08	48.85	52.34	50.33	53.49
Gemini-2.5-Flash	53.54	55.48	55.47	55.76	1.02	54.57	53.60	57.36	58.14	49.24
QvQ-72B-Preview	48.00	46.73	42.32	45.23	2.12	45.18	47.62	48.32	44.08	47.98
GPT-4-Turbo-V	47.47	45.51	46.88	46.34	0.83	46.83	43.48	50.65	49.17	51.52
GPT-4o	47.30	45.18	40.23	45.35	3.01	45.52	43.27	48.58	47.51	51.52
GPT-4o-mini	35.16	36.21	32.42	33.09	1.77	35.26	34.31	34.88	34.55	29.55
Claude-3.7-Sonnet	49.41	48.01	51.56	50.68	1.55	50.75	49.11	49.10	49.83	46.21
Qwen2.5-VL-72B-Instruct	42.72	41.14	42.71	43.66	0.90	40.95	43.52	42.64	45.07	44.70
MedGemma-27b-it	43.73	44.80	46.88	48.08	1.70	47.64	43.03	44.10	43.19	54.08

Table 3: **Accuracy (%) of Models by Frame Count and Modality on MEDFRAMEQA.** We report the accuracy of models on questions in MEDFRAMEQA grouped by frame count with standard deviation (*SD*) and by modality. We empirically observe that accuracy fluctuates with increasing frame count and varies significantly across common imaging modalities.

3.5 Data Filtering

Difficulty Filtering. To ensure difficulty, we filtered using GPT-4-Turbo-V (OpenAI, 2023b), o1 (Jaech et al., 2024), and GPT-4o (Hurst et al., 2024). We discarded items where all models reached a consensus (either *all* correct or *all* identically incorrect) to eliminate trivial or potentially erroneous keys. This step trims the pool from 4,457 to 3,654 items.

Human Evaluation. We manually filtered the dataset to ensure quality and privacy, excluding 803 entries containing blurred frames, recognizable faces, or insignificant medical content. This yielded final 2,851 high-quality entries.

4 Experiments

4.1 Data Statistics

In this section we summarize the data distribution of MEDFRAMEQA. Starting from the 3,420 instructional videos collected in Section 3.1, we extract 111,942 key-frames and retain 9,237 high-quality, medically relevant frames. These frames are used to construct 2,851 multi-image, closed-ended, single-choice VQA pairs, which span 9 human body systems and 43 organs, featuring 114 unique keyword combinations following Herring (2019). Each generated VQA pair consists of 2–5 frames, accompanied by a challenging question that requires integrating information across all provided frames to answer correctly. The composition of body systems, organs and modalities in MEDFRAMEQA is provided in Section B and shown in Figure 5 (a) (b) (c) respectively.

A defining feature of MEDFRAMEQA is that

every question is tethered to multiple images, deliberately pushing models to reason across frames—a core requirement in real-world diagnosis. Concretely, among the 2,851 VQA items, 1,186 pairs contain 2 frames, 602 pairs contain 3 frames, 256 pairs contain 4 frames, and 807 pairs contain 5 frames. We also present the distribution of frames per question in Figure 5(e).

4.2 Models

We evaluate both proprietary and open-source MLLMs on MEDFRAMEQA, encompassing reasoning and non-reasoning models, with a particular focus on recent advancements in medical reasoning. For evaluation, we use the prompt template as in MMMU-pro (Yue et al., 2024b) (see Section F).

Reasoning Models: We evaluate both proprietary reasoning model and open-source reasoning model, including 4 proprietary models o4-mini (OpenAI, 2025), o3 (OpenAI, 2025), o1 (Jaech et al., 2024), Claude-3.7-Sonnet (Anthropic, 2025) and Gemini-2.5-Flash (Google, 2025) and one open-source QvQ-72B-Preview (Team, 2024).

Non-Reasoning Models: We evaluate MEDFRAMEQA on non-reasoning models, including 3 proprietary models, GPT-4o (Hurst et al., 2024), GPT-4o-mini (Hurst et al., 2024) and GPT-4-Turbo-V (OpenAI, 2023b) and 2 open-source models Qwen2.5-VL-72B-Instruct (Bai et al., 2025) and the medical fine-tuned model MedGemma-27b-it (Sellergren et al., 2025b) to evaluate domain-specific adaptations.

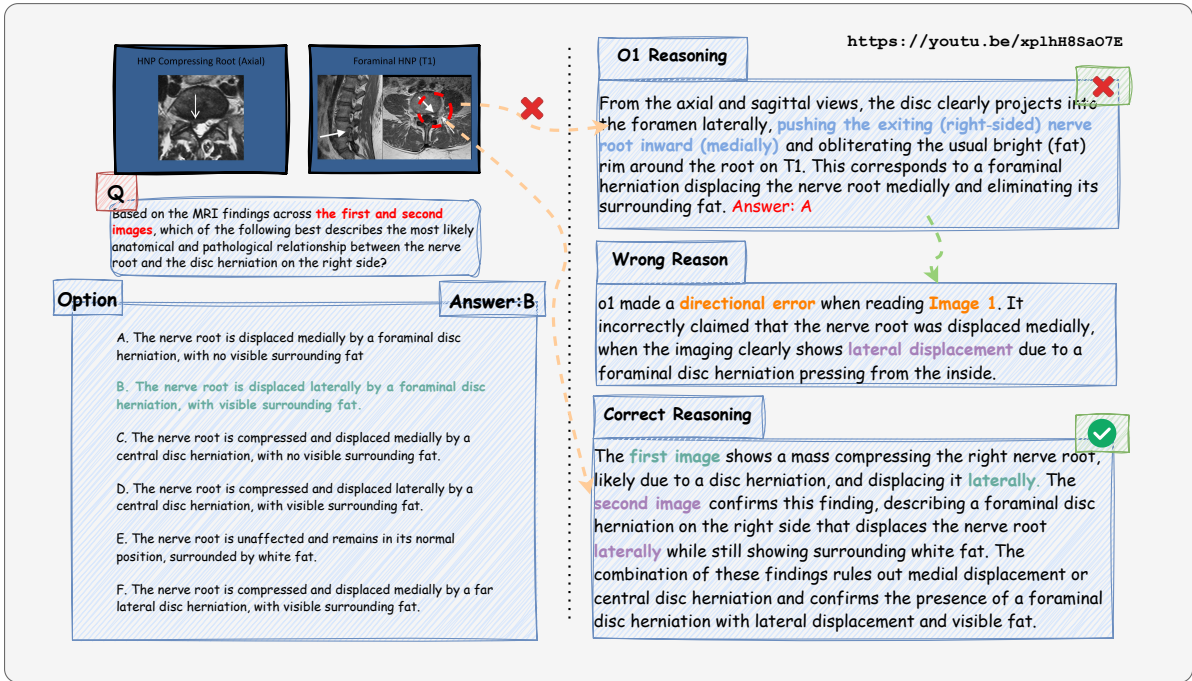


Figure 3: **Failure case study of o1 on MEDFRAMEQA.** A single image mistake can cause significant errors. Here, o1 made a directional error when interpreting the first frame, which propagated through its reasoning process and ultimately led to an incorrect answer.

4.3 Main Results

Advanced MLLMs struggle to holistically understand multi-images. Table 2 presents the evaluation of 11 advanced MLLMs on MEDFRAMEQA. In general, all assessed models demonstrate persistently low accuracy, with the peak accuracy remaining below 55.00%.

The proprietary model, GPT-4o, reaches an average accuracy of 45.67%, significantly lower in comparison to its performance on the single medical VQA benchmark (69.91% on VQA-RAD (Lau et al., 2018) as reported by Yan et al. (2024)). The leading open-source model, Qwen2.5-VL-72B-Instruct, achieves merely $42.65 \pm 0.34\%$ (SE) accuracy. To confirm this stemmed from reasoning deficits rather than inadequate medical knowledge, we evaluated MedGemma-27b-it, which similarly yielded poor results with $45.47 \pm 0.59\%$ (SE) accuracy.

Reasoning enhances multi-image understanding. As shown in Table 2, we find that reasoning MLLMs consistently outperform non-reasoning ones. Gemini-2.5-Flash attains the highest accuracy among all models, notably outperforming the top non-reasoning model GPT-4o by 9.08% (54.75% vs 45.67%). Among the open-source models, QvQ-72B-Preview achieves an accuracy

of $46.44\% \pm 0.66\%$ (SE), showcasing a 3.79% enhancement compared to its non-reasoning counterpart, Qwen2.5-VL-72B-Instruct. This indicates that reasoning is particularly beneficial in clinical scenarios, which frequently involve interpreting multiple images.

Overlooking or misinterpreting hinders reasoning across image sequence. Despite the relatively enhanced performance of reasoning models, their performance is still limited. Our investigation reveals this primarily arises from neglecting or misinterpreting the intermediary images during continuous reasoning over an image sequence. Here, we present a case study highlighting instances where o1 fails to provide correct reasoning steps for questions in MEDFRAMEQA:

Case 1: Negligence of important information within multiple frames. In Figure 4, o1 fails to integrate important information across multiple frames, leading to a flawed overall reasoning. While o1 correctly identifies the “polar vessel sign” in the Doppler frame as suggestive of a parathyroid adenoma, it ignores distinct transverse and sagittal localization cues (posterior–inferior to the thyroid with specific cranial–caudal orientation), leading to an incorrect conclusion.

Case 2: Mistake drawn from single image resulting in significant errors in subsequent reasoning. In

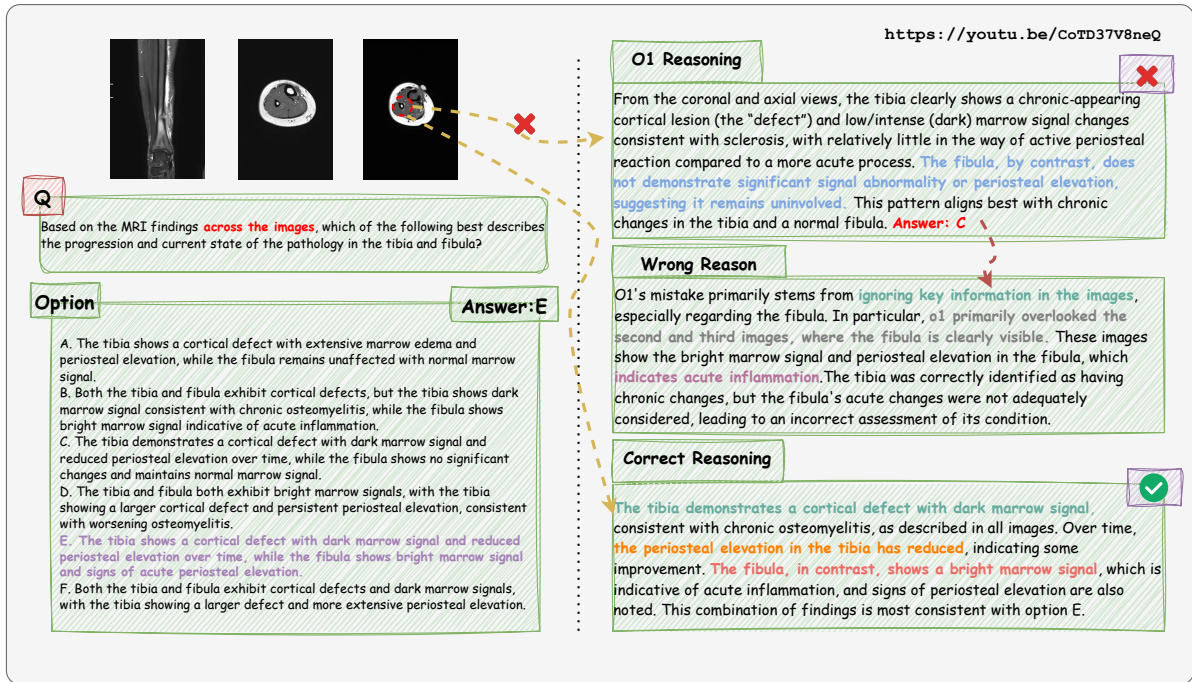


Figure 4: **Failure case study of o1 on MEDFRAMEQA.** Negligence of important information across multiple frames. In this case, o1 overlooked critical features in the second and third frames, which ultimately led to the selection of an incorrect answer.

Figure 3, o1 misreads a critical axial frame, incorrectly identifying medial rather than lateral nerve root displacement caused by a foraminal disc herniation. This error propagates through the reasoning process, yielding an anatomically incorrect answer that conflicts with evidence from both frames.

4.4 Evaluation across anatomical structures or frame numbers

Comparisons between anatomical structures and modalities. The system-wise performance we report in Table 2 reveals substantial variability in task difficulty. For instance, Gemini-2.5-Flash achieves an accuracy of 60.21% on questions related to the musculoskeletal system, but only 48.61% on the urinary system, resulting in 11.60% gap. In Section E, we present a detailed analysis of performance variation across four representative organs in MEDFRAMEQA. We also report the performance of MLLMs across different imaging modalities in Table 3. Notably, the accuracy varies significantly across common modalities such as CT, MRI, Ultrasound, and X-ray. QvQ-72B-Preview exhibits a 4.24% performance gap between Ultrasound and X-ray, whereas Gemini-2.5-Flash shows a 4.54% gap between MRI and X-ray, underscoring the strong modality sensitivity of current MLLMs and indicating the need for more diverse

and balanced modality–organ combinations during training to improve generalization.

Comparisons between VQAs with different numbers of frames. In Table 3, we report the accuracy of models on questions in MEDFRAMEQA, grouped by the number of frames each question contains. Empirically, we observe that accuracy fluctuates as the number of images per question increases, with performance improving at certain frame counts and declining at others. Among the MLLMs, GPT-4o exhibits substantial fluctuation, with a standard deviation of 3.01, whereas GPT-4-Turbo-V shows minimal variation, with a standard deviation of just 0.83. These fluctuations suggest that performance depends less on the number of frames than on the complexity or redundancy of visual information across them.

5 Conclusion

We introduces MEDFRAMEQA, a multi-image medical visual question answering benchmark, comprising 2851 multi-image questions, sourced from 3420 medical videos of 114 keywords and covering over 43 organs. We propose an automated pipeline to generate high-quality multi-image VQA data ensuring semantic progression and contextual consistency across frames. Unlike existing single-image datasets, MEDFRAMEQA has both multi-

image question answering pairs and a detailed reasoning process, containing 2-5 images input and 3.24 images input per question. We comprehensively benchmark ten state-of-the-art models, presenting accuracies predominantly below 50%. We hope MEDFRAMEQA paves the way for future multi-modal medical reasoning research.

Limitations

A key limitation is that MEDFRAMEQA has not received full-scale physician evaluation. We only obtained clinician review for a subset of questions, and the feedback on this subset indicated the questions are overall quite good. Nevertheless, broader expert assessment is needed to further verify clinical correctness and coverage. While MEDFRAMEQA reveals clear evidence of current MLLMs' inability in handling multi-image questions of clinical reasoning, effective strategies to enhance their multi-image reasoning capabilities remain underexplored. Future work will focus on developing and evaluating methods to improve such capabilities. We believe MEDFRAMEQA will serve as a valuable resource for advancing research in multimodal medical AI and fostering the development of more capable and robust diagnostic reasoning systems.

Ethical Considerations

The MedFrameQA benchmark was constructed exclusively using publicly available medical education videos hosted on YouTube. This study did not involve the recruitment of human subjects, direct interaction with patients, or the collection of private clinical data. To strictly uphold data privacy and ethical standards, a comprehensive multi-stage filtering protocol was implemented. All extracted video frames were subjected to both automated screening via GPT-4o and rigorous manual review to ensure the complete removal of personally identifiable information. Specifically, any frames containing recognizable human faces, including those of patients or video presenters, were excluded from the dataset. The final dataset consists solely of de-identified medical imagery derived from open-access educational content, ensuring compliance with privacy norms while fostering the development of robust clinical AI systems.

Acknowledgments

We thank the Microsoft Accelerate Foundation Models Research Program for supporting our computing needs.

References

- Martin Gameli Akakpo and Patrick Kafui Akakpo. 2024. [Recognizing the role of youtube in medical education](#). *Discover Education*, 3(1):73.
- Rawan AlSaad, Alaa Abd-Alrazaq, Sabri Boughorbel, Arfan Ahmed, Max-Antoine Renault, Rafat Damseh, and Javaid Sheikh. 2024. [Multimodal large language models in health care: Applications, challenges, and future outlook](#). *Journal of Medical Internet Research*, 26:e59505. Epub ahead of print.
- Anthropic. 2025. Claude 3.7 sonnet and claude code. <https://www.anthropic.com/news/claude-3-7-sonnet>.
- Shuai Bai, Keqin Chen, Xuejing Liu, Jialin Wang, Wenbin Ge, Sibao Song, Kai Dang, Peng Wang, Shijie Wang, Jun Tang, Humen Zhong, Yuanzhi Zhu, Ming-Hsuan Yang, Zhaohai Li, Jianqiang Wan, Pengfei Wang, Wei Ding, Zheren Fu, Yiheng Xu, and 8 others. 2025. [Qwen2.5-vl technical report](#). *CoRR*, abs/2502.13923.
- Asma Ben Abacha, Sadid A. Hasan, Vivek V. Datla, Joey Liu, Dina Demner-Fushman, and Henning Müller. 2019. [Vqa-med: Overview of the medical visual question answering task at imageclef 2019](#). In *Working Notes of CLEF 2019*, volume 2380 of *CEUR Workshop Proceedings*, Lugano, Switzerland. CEUR-WS.org.
- Asma Ben Abacha, Mourad Sarrouiti, Dina Demner-Fushman, Sadid A. Hasan, and Henning Müller. 2021. Overview of the vqa-med task at imageclef 2021: Visual question answering and generation in the medical domain. In *CLEF 2021 Working Notes*, CEUR Workshop Proceedings, Bucharest, Romania. CEUR-WS.org.
- Hardy Chen, Haoqin Tu, Fali Wang, Hui Liu, Xianfeng Tang, Xinya Du, Yuyin Zhou, and Cihang Xie. 2025. Sft or rl? an early investigation into training rl-like reasoning large vision-language models. *arXiv preprint arXiv:2504.11468*.
- Pengcheng Chen, Jin Ye, Guoan Wang, Yanjun Li, Zhongying Deng, Wei Li, Tianbin Li, Haodong Duan, Ziyang Huang, Yanzhou Su, Benyou Wang, Shaoting Zhang, Bin Fu, Jianfei Cai, Bohan Zhuang, Eric J. Seibel, Junjun He, and Yu Qiao. 2024. [Gmailmmbench: A comprehensive multimodal evaluation benchmark towards general medical AI](#). In *Advances in Neural Information Processing Systems 38: Annual Conference on Neural Information Processing Systems 2024, NeurIPS 2024, Vancouver, BC, Canada, December 10 - 15, 2024*.

- Yihe Deng, Hritik Bansal, Fan Yin, Nanyun Peng, Wei Wang, and Kai-Wei Chang. 2025. Openvlthinker: An early exploration to complex vision-language reasoning via iterative self-improvement. *arXiv preprint arXiv:2503.17352*.
- Adeeb Derakhshan, Linda Lee, Prabhat Bhamra, Eric Barbarite, and David Shaye. 2019. Assessing the educational quality of 'youtube' videos for facelifts. *American Journal of Otolaryngology*, 40(2):156–159. Epub 2019 Jan 4.
- Negin Ghamsarian, Yosuf El-Shabrawi, Sahar Nasir-ihaghighi, Doris Putzgruber-Adamitsch, Martin Zinkernagel, Sebastian Wolf, Klaus Schoeffmann, and Raphael Sznitman. 2024. Cataract-1k dataset for deep-learning-assisted analysis of cataract surgery videos. *Scientific Data*, 11(1):373.
- Google. 2025. Start building with gemini 2.5 flash. <https://developers.googleblog.com/en/start-building-with-gemini-25-flash/>.
- Deepak Gupta, Kush Attal, and Dina Demner-Fushman. 2023. A dataset for medical instructional video classification and question answering. *Scientific Data*, 10(1):158.
- Xuehai He, Yichen Zhang, Luntian Mou, Eric P. Xing, and Pengtao Xie. 2020. Pathvqa: 30000+ questions for medical visual question answering. *CoRR*, abs/2003.10286.
- William Herring. 2019. *Learning radiology: recognizing the basics*. Elsevier Health Sciences.
- Ming Hu, Lin Wang, Siyuan Yan, Don Ma, Qingli Ren, Peng Xia, Wei Feng, Peibo Duan, Lie Ju, and Zongyuan Ge. 2023. Nurvid: A large expert-level video database for nursing procedure activity understanding. In *Advances in Neural Information Processing Systems 36: Annual Conference on Neural Information Processing Systems 2023, NeurIPS 2023, New Orleans, LA, USA, December 10 - 16, 2023*.
- Yutao Hu, Tianbin Li, Quanfeng Lu, Wenqi Shao, Junjun He, Yu Qiao, and Ping Luo. 2024. Omnimedvqa: A new large-scale comprehensive evaluation benchmark for medical LVLm. In *IEEE/CVF Conference on Computer Vision and Pattern Recognition, CVPR 2024, Seattle, WA, USA, June 16-22, 2024*, pages 22170–22183. IEEE.
- Xiaoke Huang, Juncheng Wu, Hui Liu, Xianfeng Tang, and Yuyin Zhou. 2025. m1: Unleash the potential of test-time scaling for medical reasoning with large language models. *arXiv preprint arXiv:2504.00869*.
- Aaron Hurst, Adam Lerer, Adam P. Goucher, Adam Perelman, Aditya Ramesh, Aidan Clark, AJ Ostrow, Akila Welihinda, Alan Hayes, Alec Radford, Aleksander Madry, Alex Baker-Whitcomb, Alex Beutel, Alex Borzunov, Alex Carney, Alex Chow, Alex Kirillov, Alex Nichol, Alex Paino, and 79 others. 2024. Gpt-4o system card. *CoRR*, abs/2410.21276.
- Wisdom Oluchi Ikezogwo, Mehmet Saygin Seyfioglu, Fatemeh Ghezloo, Dylan Stefan Chan Geva, Fatwir Sheikh Mohammed, Pavan Kumar Anand, Ranjay Krishna, and Linda G. Shapiro. 2023. Quilt-1m: One million image-text pairs for histopathology. In *Advances in Neural Information Processing Systems 36: Annual Conference on Neural Information Processing Systems 2023, NeurIPS 2023, New Orleans, LA, USA, December 10 - 16, 2023*.
- Aaron Jaech, Adam Kalai, Adam Lerer, Adam Richardson, Ahmed El-Kishky, Aiden Low, Alec Helvar, Aleksander Madry, Alex Beutel, Alex Carney, Alex Iftimie, Alex Karpenko, Alex Tachard Passos, Alexander Neitz, Alexander Prokofiev, Alexander Wei, Allison Tam, Ally Bennett, Ananya Kumar, and 80 others. 2024. Openai o1 system card. *CoRR*, abs/2412.16720.
- Songtao Jiang, Yuan Wang, Sibao Song, Tianxiang Hu, Chenyi Zhou, Bin Pu, Yan Zhang, Zhibo Yang, Yang Feng, Joey Tianyi Zhou, and 1 others. 2025. Hulumed: A transparent generalist model towards holistic medical vision-language understanding. *arXiv preprint arXiv:2510.08668*.
- Joseph Lau, Swagata Gayen, Asma Ben Abacha, and Dina Demner-Fushman. 2018. A dataset of clinically generated visual questions and answers about radiology images. *Scientific Data*, 5:180251.
- Chunyu Li, Cliff Wong, Sheng Zhang, Naoto Usuyama, Haotian Liu, Jianwei Yang, Tristan Naumann, Hoifung Poon, and Jianfeng Gao. 2023. Llavamed: Training a large language-and-vision assistant for biomedicine in one day. In *Advances in Neural Information Processing Systems 36: Annual Conference on Neural Information Processing Systems 2023, NeurIPS 2023, New Orleans, LA, USA, December 10 - 16, 2023*.
- Bo Liu, Li-Ming Zhan, Li Xu, Lin Ma, Yan Yang, and Xiao-Ming Wu. 2021. Slake: A semantically-labeled knowledge-enhanced dataset for medical visual question answering. In *18th IEEE International Symposium on Biomedical Imaging, ISBI 2021, Nice, France, April 13-16, 2021*, pages 1650–1654. IEEE.
- OpenAI. 2023a. GPT-4 technical report. *CoRR*, abs/2303.08774.
- OpenAI. 2023b. GPT-4V(ision) system card. *OpenAI*.
- OpenAI. 2025. Introducing o3 and o4 mini. <https://openai.com/index/introducing-o3-and-o4-mini/>.
- Wafa Osman, Faiza Mohamed, Mohamed Elhassan, and Abdelilah Shoufan. 2022. Is youtube a reliable source of health-related information? a systematic review. *BMC Medical Education*, 22(1):382.
- Jiazhen Pan, Che Liu, Junde Wu, Fenglin Liu, Jiayuan Zhu, Hongwei Bran Li, Chen Chen, Cheng Ouyang, and Daniel Rueckert. 2025. Medvlm-r1: Incentivizing medical reasoning capability of vision-language

- models (vlms) via reinforcement learning. *CoRR*, abs/2502.19634.
- Alec Radford, Jong Wook Kim, Tao Xu, Greg Brockman, Christine McLeavey, and Ilya Sutskever. 2023. [Robust speech recognition via large-scale weak supervision](#). In *International Conference on Machine Learning, ICML 2023, 23-29 July 2023, Honolulu, Hawaii, USA*, volume 202 of *Proceedings of Machine Learning Research*, pages 28492–28518. PMLR.
- Khaled Saab, Tao Tu, Wei-Hung Weng, Ryutaro Tanno, David Stutz, Ellery Wulczyn, Fan Zhang, Tim Strother, Chunjong Park, Elahe Vedadi, Juanma Zambrano Chaves, Szu-Yeu Hu, Mike Schaekermann, Aishwarya Kamath, Yong Cheng, David G. T. Barrett, Cathy Cheung, Basil Mustafa, Anil Palepu, and 48 others. 2024. [Capabilities of gemini models in medicine](#). *CoRR*, abs/2404.18416.
- Andrew Sellergren, Sahar Kazemzadeh, Tiam Jaroensri, Atilla Kiraly, Madeleine Traverse, Timo Kohlberger, Shawn Xu, Fayaz Jamil, Cían Hughes, Charles Lau, and 1 others. 2025a. [Medgemma technical report](#). *arXiv preprint arXiv:2507.05201*.
- Andrew Sellergren, Sahar Kazemzadeh, Tiam Jaroensri, Atilla P. Kiraly, Madeleine Traverse, Timo Kohlberger, Shawn Xu, Fayaz Jamil, Cían Hughes, Charles Lau, Justin Chen, Fereshteh Mahvar, Liron Yatziv, Tiffany Chen, Bram Sterling, Stefanie Anna Baby, Susanna Maria Baby, Jeremy Lai, Samuel Schmidgall, and 62 others. 2025b. [Medgemma technical report](#). *CoRR*, abs/2507.05201.
- Q. Team. 2024. [Qvq: To see the world with wisdom](#). <https://qwmlm.github.io/blog/qvq-72b-preview/>.
- Tao Tu, Shekoofeh Azizi, Danny Driess, Mike Schaekermann, Mohamed Amin, Pi-Chuan Chang, Andrew Carroll, Chuck Lau, Ryutaro Tanno, Ira Ktena, Basil Mustafa, Aakanksha Chowdhery, Yun Liu, Simon Kornblith, David J. Fleet, Philip Andrew Mansfield, Sushant Prakash, Renee Wong, Sunny Virmani, and 13 others. 2023. [Towards generalist biomedical AI](#). *CoRR*, abs/2307.14334.
- Yaoting Wang, Shengqiong Wu, Yuecheng Zhang, Shuicheng Yan, Ziwei Liu, Jiebo Luo, and Hao Fei. 2025. [Multimodal chain-of-thought reasoning: A comprehensive survey](#). *CoRR*, abs/2503.12605.
- Yiqi Wang, Wentao Chen, Xiaotian Han, Xudong Lin, Haiteng Zhao, Yongfei Liu, Bohan Zhai, Jianbo Yuan, Quanzeng You, and Hongxia Yang. 2024. [Exploring the reasoning abilities of multimodal large language models \(mlms\): A comprehensive survey on emerging trends in multimodal reasoning](#). *CoRR*, abs/2401.06805.
- Juncheng Wu, Wenlong Deng, Xingxuan Li, Sheng Liu, Taomian Mi, Yifan Peng, Ziyang Xu, Yi Liu, Hyunjin Cho, Chang-In Choi, and 1 others. 2025. [Medreason: Eliciting factual medical reasoning steps in llms via knowledge graphs](#). *arXiv preprint arXiv:2504.00993*.
- Yunfei Xie, Juncheng Wu, Haoqin Tu, Siwei Yang, Bingchen Zhao, Yongshuo Zong, Qiao Jin, Cihang Xie, and Yuyin Zhou. 2024. [A preliminary study of o1 in medicine: Are we closer to an ai doctor?](#) *arXiv preprint arXiv:2409.15277*.
- Yunfei Xie, Ce Zhou, Lang Gao, Juncheng Wu, Xianhang Li, Hong-Yu Zhou, Sheng Liu, Lei Xing, James Zou, Cihang Xie, and Yuyin Zhou. 2025. [Medtrinity-25m: A large-scale multimodal dataset with multi-granular annotations for medicine](#). In *The Thirteenth International Conference on Learning Representations*.
- Qianqi Yan, Xuehai He, Xiang Yue, and Xin Eric Wang. 2024. [Worse than random? an embarrassingly simple probing evaluation of large multimodal models in medical vqa](#). *arXiv preprint arXiv:2405.20421*.
- Xiang Yue, Yuansheng Ni, Tianyu Zheng, Kai Zhang, Ruoqi Liu, Ge Zhang, Samuel Stevens, Dongfu Jiang, Weiming Ren, Yuxuan Sun, Cong Wei, Botao Yu, Ruibin Yuan, Renliang Sun, Ming Yin, Boyuan Zheng, Zhenzhu Yang, Yibo Liu, Wenhao Huang, and 3 others. 2024a. [MMMU: A massive multi-discipline multimodal understanding and reasoning benchmark for expert AGI](#). In *IEEE/CVF Conference on Computer Vision and Pattern Recognition, CVPR 2024, Seattle, WA, USA, June 16-22, 2024*, pages 9556–9567. IEEE.
- Xiang Yue, Tianyu Zheng, Yuansheng Ni, Yubo Wang, Kai Zhang, Shengbang Tong, Yuxuan Sun, Botao Yu, Ge Zhang, Huan Sun, Yu Su, Wenhao Chen, and Graham Neubig. 2024b. [Mmmu-pro: A more robust multi-discipline multimodal understanding benchmark](#). *CoRR*, abs/2409.02813.
- Xiaoman Zhang, Chaoyi Wu, Ziheng Zhao, Weixiong Lin, Ya Zhang, Yanfeng Wang, and Weidi Xie. 2023. [PMC-VQA: visual instruction tuning for medical visual question answering](#). *CoRR*, abs/2305.10415.
- Yuxin Zuo, Shang Qu, Yifei Li, Zhangren Chen, Xuekai Zhu, Ermo Hua, Kaiyan Zhang, Ning Ding, and Bowen Zhou. 2025. [Medxpertqa: Benchmarking expert-level medical reasoning and understanding](#). *CoRR*, abs/2501.18362.

A Use of LLMs

We employed large language models (LLMs) in the dataset construction pipeline to refine and filter captions, identify and merge semantically related captions, and generate multi-image VQA items. We further benchmarked state-of-the-art MLLMs on MedFrameQA.

During the preparation of this manuscript, we used OpenAI’s GPT-4.1 model for minor language refinement and smoothing of the writing. The AI tool was not used for generating original content, conducting data analysis, or formulating core scientific ideas. All conceptual development, experimentation, and interpretation were conducted independently without reliance on AI tools.

B Data Distribution

We present detailed data distributions across body systems, organs, and imaging modalities in Figure 5(a), (b), and (c), respectively. A word cloud of keywords in MEDFRAMEQA is shown in Figure 5(d), and the distribution of frame counts per question is provided in Figure 5(e).

C API Cost

Generation of each data entry costs 5 times calling of GPT-4o API on average, depending on the number of frames involved in the data entry. Construction of 2,851 data entries costs 14,255 API calls in total.

For proprietary models (e.g., GPT-4o, Gemini-2.5-Flash, Claude-3.7-Sonnet), we use their official APIs and perform 2,851 requests per model, corresponding to the number of examples in MEDFRAMEQA.

For open-source models (e.g., QvQ-72B-Preview, Qwen2.5-VL-72B-Instruct, MedGemma-27b-it), we conducted three independent runs on 4xA100 GPUs and calculated error bars. Due to API quota constraints, proprietary models were evaluated only once.

D Keyword List

We present comprehensive list of search queries utilized for video collection. As detailed in Section 3.1, we curated a total of 114 combinatorial search queries to ensure broad coverage of routine diagnostic scenarios. Each query is formed by pairing a specific imaging modality (e.g., MRI, X-Ray, CT) with a frequently encountered clinical disease. These keywords, listed in Figure 6 and Figure 7, span 9 human body systems and 43 organs, serving as the foundational criteria for retrieving high-quality medical educational videos from YouTube.

System	Organ	Keyword
central nervous system	brain	stroke CT brain tumor MRI cerebral hemorrhage CT epilepsy EEG imaging traumatic brain injury CT
	spinal cord	spinal cord injury MRI disc herniation MRI spinal stenosis CT myelitis MRI
respiratory system	lung	pneumonia chest radiograph lung cancer CT pulmonary embolism CT angiography chronic obstructive pulmonary disease CT
	trachea bronchi	bronchial asthma bronchography
	pleura	pleural effusion ultrasound
circulatory system	heart	coronary artery disease angiography heart failure echocardiography myocardial infarction CT cardiomyopathy MRI
	pulmonary arteries	pulmonary embolism CT angiography pulmonary hypertension CT
	aorta	aortic aneurysm CT aortic dissection MR angiography
digestive system	esophagus	esophageal cancer CT gastroesophageal reflux esophagram esophageal stricture endoscopic ultrasound
	stomach	gastric cancer CT peptic ulcer gastroscopy gastritis upper gastrointestinal series
	liver	liver cirrhosis CT hepatocellular carcinoma MRI hepatitis ultrasound
	pancreas	pancreatic cancer CT acute pancreatitis CT chronic pancreatitis MRCP
	gallbladder	gallstones ultrasound cholecystitis HIDA scan gallbladder cancer CT
	small intestine	Crohn's disease MRI enterography small bowel obstruction CT intestinal bleeding capsule endoscopy
	large intestine	colorectal cancer colonoscopy diverticulitis CT ulcerative colitis barium enema
urinary system	kidneys	kidney stones CT renal cell carcinoma MRI pyelonephritis ultrasound
	ureters	ureteral stones CT urography ureteral stricture MR urography
	bladder	bladder cancer cystoscopy urinary tract infection ultrasound bladder stones CT
	urethra	urethral stricture urethrography urethral injury CT urethrography
reproductive system	testes	testicular cancer ultrasound testicular torsion Doppler ultrasound epididymitis ultrasound
	prostate	prostate cancer MRI benign prostatic hyperplasia TRUS prostatitis pelvic CT

Figure 6: Keyword List (Part 1)

E Comparison of Organs

We present a detailed organ-wise accuracy comparison of 11 state-of-the-art MLLMs on MED-FRAMEQA in Table 4. Our results reveal substantial performance variation across different organs. While Gemini-2.5-Flash outperforms other models on average in Table 2, open-source models like QvQ-72B-Preview demonstrate competitive performance on specific organs, such as the ureters and pulmonary arteries. This variability highlights the sensitivity of MLLM performance to the anatomical structures involved, underscoring the need to develop models that are more robust to anatomical diversity. This variability underscores the sensitivity of MLLM performance to organ-specific features and highlights the need for future research focused on improving anatomical generalization across a wide range of clinical scenarios.

System	Organ	Keyword
	penis	erectile dysfunction Doppler ultrasound Peyronie's disease MRI
	ovaries	ovarian cyst ultrasound ovarian cancer MRI polycystic ovary syndrome ultrasound
	uterus	endometrial cancer MRI uterine fibroids ultrasound adenomyosis pelvic MRI
	cervix	cervical cancer MRI cervical dysplasia colposcopy
	vagina	vaginal cancer MRI vaginal prolapse transvaginal ultrasound
endocrine system	thyroid	thyroid nodule ultrasound thyroid cancer scintigraphy hyperthyroidism neck CT
	parathyroid	parathyroid adenoma scintigraphy hyperparathyroidism ultrasound
	adrenal glands	adrenal adenoma CT pheochromocytoma MRI Cushing's syndrome adrenal scintigraphy
	pancreas (endocrine)	insulinoma CT pancreatic neuroendocrine tumor MRI
	pituitary gland	pituitary adenoma MRI acromegaly dynamic MRI
	hypothalamus	hypothalamic tumor MRI hypopituitarism functional MRI
musculoskeletal system	bones	osteoporosis DEXA bone fracture radiograph osteomyelitis MRI
	joints	osteoarthritis radiograph rheumatoid arthritis MRI joint effusion ultrasound
	skeletal muscles	muscle tear MRI myositis ultrasound muscular dystrophy EMG imaging
	spine	disc herniation MRI spinal stenosis CT spondylolisthesis radiograph
auxiliary systems and tissues	eyes	glaucoma OCT retinal detachment ultrasound macular degeneration fundus photography
	ears	otitis media temporal bone CT hearing loss brain MRI
	skin	melanoma confocal microscopy skin cancer dermatologic ultrasound
	lymph nodes	lymphoma CT lymphadenitis ultrasound
	soft tissues	soft tissue sarcoma MRI lipoma ultrasound
	salivary glands	salivary gland tumor ultrasound sialadenitis sialography
	breast	breast cancer mammography fibroadenoma ultrasound breast cyst MRI

Figure 7: Keyword List (Part 2)

Organs	Model Accuracy										
	Gemini-2.5-Flash	Claude-3.7-Sonnet	o4-mini	o3	o1	GPT-4o	GPT-4o-mini	GPT-4-Turbo-V	QvQ-72B	Qwen2.5-VL-72B-Instruct	MedGemma-27b-it
auxiliary systems and tissues											
soft tissues	48.65	37.84	45.95	39.19	35.14	36.49	32.43	35.14	40.54	30.63	35.68
salivary glands	55.00	50.00	45.00	52.63	47.37	40.00	40.00	45.00	66.67	48.33	43.33
skin	33.33	66.67	50.00	70.00	54.55	75.00	41.67	75.00	36.11	63.89	50.00
breast	52.63	55.26	55.26	57.89	58.33	42.11	39.47	39.47	50.88	35.09	41.23
lymph nodes	61.11	77.78	72.22	72.22	61.11	55.56	27.78	61.11	53.70	55.56	53.70
ears	58.33	47.22	44.44	52.78	57.14	50.00	30.56	55.56	46.30	37.04	40.74
eyes	56.25	50.00	54.17	46.81	51.06	43.75	37.50	52.08	47.22	45.83	36.11
central nervous system											
brain	50.00	49.38	42.41	45.86	46.05	51.25	44.38	46.88	42.92	42.50	51.87
spinal cord	46.81	48.94	52.13	51.06	48.35	44.68	37.23	42.55	48.23	44.33	45.74
circulatory system											
pulmonary arteries	54.84	56.99	50.54	49.46	51.09	43.01	44.09	47.31	51.97	44.09	49.82
aorta	60.81	48.65	45.21	50.00	45.83	35.14	35.14	41.89	43.69	40.09	52.70
heart	55.88	52.94	51.52	51.52	53.12	26.47	35.29	32.35	43.14	42.16	37.25
digestive system											
large intestine	47.29	47.29	42.64	38.28	41.73	48.06	23.26	46.51	35.14	31.52	37.98
esophagus	59.26	51.85	70.37	62.96	59.26	62.96	22.22	62.96	61.73	38.27	60.49
small intestine	61.11	55.56	72.22	58.82	62.50	44.44	16.67	55.56	46.30	50.00	55.56
gallbladder	37.70	44.26	34.43	38.33	41.38	40.98	39.34	47.54	40.98	36.61	39.34
stomach	59.09	59.09	55.17	60.00	54.12	57.95	32.95	56.82	37.88	51.14	46.59
liver	54.90	54.90	52.94	60.78	52.94	50.98	29.41	43.14	54.25	46.41	43.14
pancreas	39.29	35.71	42.86	39.29	35.71	42.86	25.00	42.86	32.14	32.14	44.05
endocrine system											
pancreas (endocrine)	41.18	35.29	52.94	35.29	35.29	41.18	17.65	41.18	35.29	25.49	29.41
hypothalamus	56.67	43.33	53.85	50.00	42.31	46.67	43.33	46.67	45.56	45.56	52.22
parathyroid	56.41	38.46	47.37	50.00	57.14	41.03	35.90	46.15	49.57	47.86	60.68
pituitary gland	56.34	56.34	59.15	57.75	56.52	45.07	21.13	47.89	57.28	52.11	54.93
adrenal glands	53.12	43.75	53.12	43.75	25.00	53.12	40.62	43.75	41.67	27.08	45.83
thyroid	58.06	51.61	46.77	55.74	50.00	48.39	30.65	61.29	43.01	41.40	45.70
musculoskeletal system											
spine	57.14	49.11	48.21	58.04	48.65	47.32	35.71	50.00	48.81	46.43	48.51
bones	62.68	50.70	51.77	56.83	54.07	43.66	37.32	38.03	55.16	40.38	41.31
skeletal muscles	63.55	61.68	62.62	54.29	50.94	45.79	38.32	51.40	50.78	56.39	57.63
joints	58.53	50.69	52.53	52.31	51.87	40.55	31.34	44.24	45.16	39.02	41.01
reproductive system											
vagina	56.88	50.46	44.44	47.17	38.24	49.54	35.78	54.13	48.01	43.12	52.60
penis	42.86	28.57	28.57	14.29	14.29	42.86	28.57	50.00	38.10	52.38	45.24
ovaries	50.79	47.62	44.44	46.77	52.54	42.86	22.22	38.10	49.74	55.03	47.62
prostate	50.63	49.37	40.51	42.86	30.26	46.84	43.04	48.10	40.93	39.66	45.57
cervix	61.29	53.23	41.67	38.98	47.37	48.39	32.26	48.39	44.09	40.32	40.32
testes	64.20	46.91	46.91	51.25	52.50	44.44	34.57	45.68	54.73	43.21	44.44
uterus	52.31	40.00	46.15	46.88	42.19	41.54	32.31	53.85	45.13	38.46	45.64
respiratory system											
trachea bronchi	50.00	60.00	55.56	62.50	55.56	70.00	30.00	50.00	46.67	73.33	66.67
lung	59.11	47.29	50.25	53.00	50.51	48.28	35.96	45.32	47.62	46.96	43.68
pleura	52.94	23.53	41.18	35.29	25.00	47.06	47.06	52.94	35.29	37.25	37.25
urinary system											
ureters	44.59	44.59	40.54	46.48	42.65	40.54	25.68	45.95	41.89	37.84	48.20
kidneys	50.00	51.19	58.33	50.00	54.32	50.00	38.10	46.43	44.84	40.48	34.52
urethra	52.17	43.48	60.87	43.48	40.91	21.74	47.83	26.09	52.17	49.28	36.23
bladder	51.43	57.14	54.29	65.71	54.29	51.43	42.86	40.00	51.43	36.19	46.67

Table 4: **Accuracy of Models by organs on MEDFRAMEQA.** We report the organ-wise accuracy of the models on MEDFRAMEQA. The best accuracy is highlighted in bold.

F Prompt Details

We details the specific prompts and instructions utilized throughout MEDFRAMEQA data curation pipeline. We provide the full text of the prompts for frame filtering in Figure 8, multi-frame merging in Figure 9, and question generation in Figure 10 to facilitate reproducibility. Additionally, the prompt template used for the model evaluation is presented in Figure 11.

Prompts for Filtering Non-Medical Image and Rephrasing

prompt_template:

You are given the following:

- A **keyframe image** extracted from a YouTube video retrieved using the keyword "{keyword}", which relates to the "{organ}" in the "{system}".
- The keyframe corresponds to the time interval: [{frame_start_time}, {frame_end_time}] in the video. You may assume that visual content remains stable during this period.
- A **list of caption segments**, spanning from {start_time} to {end_time} seconds, provided as a JSON array in the {caption_json_list} variable. These segments represent the spoken content near the frame's timestamp and may contain information that helps describe or interpret the keyframe image. Each caption object contains:
 - "startTime": start time in seconds
 - "endTime": end time in seconds
 - "sentence": caption content

Your Task

1. **Determine Benchmark Eligibility**:

Answer these questions to guide your reasoning:

1. Does the image prominently depict clear, authentic medical imaging relevant to "{keyword}" (e.g., sharp radiographs or scans, including multiple images if they are all visible and relevant)?
2. Is the image **primarily composed of medical imaging**, even if there are text overlays or minor visual obstructions?
3. Is the image suitable for inclusion in a medical benchmark dataset (e.g., sharp, intelligible, and relevant to medical imaging, with at least 85% of the image area consisting of meaningful medical imaging, excluding blank regions, borders, or irrelevant content)?
4. Is the image free of any unrelated human faces, including but not limited to presenters in video conference screenshots (e.g., Zoom speaker windows) or other non-medical human portraits?

2. **Faithful Rephrasing**:

- Rephrase the caption into a coherent, fluent, and high-quality medical description of the visual content of the current frame, as conveyed solely by the dialogue in the provided captions.
- The description must use precise medical terminology and reflect a medical imaging context (e.g., radiology or anatomy).
- **Include only information explicitly stated in the captions that directly relates to the current frame's visual content**, such as descriptions, identifications, observations, questions, answers, corrections, and transitional statements.
- Strictly avoid any details not present in the captions, including information from the image itself, external context, or unrelated dialogue (e.g., discussions about other frames or topics).

Output Format

Return your answer as a valid JSON object, you **should not include markdown in your output**:

```
{
  "result": "yes" | "no",
  "reason": "A concise explanation (max 50 words) for why the image is or is not suitable for the benchmark.",
  "captions": all the captions combined together,
  "rephrased_description": "A faithful and fluent rephrasing of the caption content, without hallucination."
}
```

If the image is **not** suitable for the benchmark (i.e., "result": "no"), then only return the following fields in your output, you **should not include markdown in your output**:

```
{
  "result": "no",
  "reason": "A concise explanation (max 50 words) for why the image is not suitable for the benchmark."
}
```

Figure 8: Filter and Rephrase Captions

Prompts for Pairing Related Captions

prompt_template:

You are given one or more caption segments corresponding to one or more continuous medical keyframes from a video. You do not have access to the actual images.

These caption segments come from a medical video retrieved using the keyword "{keyword}", and are related to the body part "{body_part}". Each caption describes the anatomical structures or procedural content visible in its corresponding keyframe.

Your task is to analyze the content of all caption segments and determine which segments are discussing **the same or closely related medical topic or structure** (e.g., same procedure, same organ, or same pathology). Group together all captions that appear to describe the same medical subject. Each group should represent a coherent topic or issue that could be visually identifiable in the corresponding keyframes.

Below are all the caption segments:

```
...  
{caption}  
...
```

Requirements:

- Focus only on medically or visually coherent topics.
- Do not group captions based only on linguistic similarity—there must be a medically meaningful connection.
- Each group must contain at least one caption.
- If a caption clearly describes a different topic from others, place it in its own group.
- For each group, provide a brief explanation in the reason field describing why these captions are grouped together.

Output Format:

The output must strictly follow the JSON format below (no markdown, no explanations):

```
{  
  "frames": [all the caption numbers],  
  "pairs_of_related_frames": [  
    {  
      "selected_captions": [1, 2],  
      "related_reason": "Both captions describe the insertion of a catheter into the same artery."  
    },  
    {  
      "selected_captions": [3],  
      "related_reason": "This caption describes a different procedure involving the venous system."  
    }  
  ]  
}
```

Figure 9: Transcripts Relation Check

Prompts for Generating VQA pairs

prompt_template:

Your task is to generate **expert-level, medically valuable** question that:

- Uses **every piece of visual information contained in the captions** (treat the captions only as your private description of each image).
- Demands advanced competencies such as anatomical reasoning, differential diagnosis, pathology identification, or procedural planning.
- Is grounded **solely in what can be seen on the images**. Do not add outside facts unless the finding is directly evident from the described appearance.
- Refers to each picture as “first image”, “second image”, etc. in the order implied by the captions.
- Never hints at, quotes, or mentions the captions, videos, or any textual description. All wording must make it seem as though the questioner has the images in front of them.
- Add as many plausible but misleading distractors as possible (commonly 4–6 or more). Craft the incorrect answer choices so they are commonly confused with the correct diagnosis/procedure given the depicted findings, thereby maximizing the likelihood of error for anyone who has not carefully interpreted every visual detail.
- Important: Do not generate questions that test theoretical definitions, textbook knowledge, or general medical concepts alone. Only generate questions whose answers depend on observing specific visual features explicitly described in the captions. Do not ask about general patterns like 'penumbra parameters'—instead, ask how those parameters appear in the actual image described.

Below are all the caption segments:

```
...  
{caption}  
...
```

Output Format (strict JSON structure, no markdown allowed):

```
{  
  "related_captions": ["caption_1", "caption_2", ...],  
  "mcq_questions": [  
    {  
      "question": "A medically grounded visual question requiring comparison across the provided images.",  
      "options": ["Option A", "Option B", "Option C", "Option D", ...],  
      "correct_answer": "Please select the best answer from the given options.",  
      "reasoning_chain": "A clear explanation of how the correct answer is visually derived by integrating details  
        from all related images.",  
      "supporting_segments": {  
        "caption_1": "Supporting phrase from caption_1.",  
        "caption_2": "Supporting phrase from caption_2.",  
        "...": "Add additional quotes as needed."  
      }  
    }  
  ]  
}
```

Figure 10: Multi-Frame VQA Pair Generation

Prompts for Evaluation

GPT Series & Claude & Qwen Series Prompt Template:

Answer the following multiple-choice question. Images are provided. The last line of your response should be strictly of the following format: 'Answer: **SLETTER**' (without quotes) where LETTER is one of the options. For example, if the correct answer is A, your response should be: 'Answer: A'. Think step by step before answering.

Question: {question}

Options:

{options}

Gemini Prompt Template:

Answer the following multiple-choice question. Images are provided. The last line of your response should be strictly of the following format: 'The final answer is **\$\boxed{LETTER}\$**' (without quotes) where LETTER is one of the options. For example, if the correct answer is A, your response should be: 'The final answer is **\$\boxed{A}\$**'. Think step by step before answering.

Question: {question}

Options:

{options}

QVQ Prompt Template:

Answer the following multiple-choice question. Images are provided. The last line of your response should be strictly of the following format: '**Final Answer*\n\n[\boxed{LETTER}]' (without quotes) where LETTER is one of the options. For example, if the correct answer is A, your response should be: '**Final Answer*\n\n[\boxed{A}]'. Think step by step before answering.

Question: {question}

Options:

{options}

Figure 11: Benchmark Evaluation

G Representative Examples

We provide a comprehensive visualization of representative samples from MEDFRAMEQA. Figures Figure 12 through Figure 15 showcase VQA pairs organized by varying input number of images, explicitly covering cases with two, three, four, and five frames respectively. Each example displays the full multi-image input sequence alongside the associated clinical question and the ground-truth answer and reasoning process. These samples highlight the complex spatial-temporal reasoning required to solve questions across different frame counts, distinguishing our benchmark from traditional single-image datasets.

Example - #1

System: respiratory system

Organ: lung

Modality: X-ray

YouTube Link: <https://youtu.be/J1n2mJ00xKs>

.....
Input Images:



Question:

Based on the radiographic findings in the first and second images, which of the following best describes the side and severity of the pneumothorax, as well as the associated mediastinal shift?

Options:

- A. A large left-sided pneumothorax with mediastinal shift to the right, as seen in the first image, and a large right-sided pneumothorax with mediastinal shift to the left, as seen in the second image.
 - B. A small left-sided pneumothorax with no mediastinal shift in the first image, and a large right-sided pneumothorax with mediastinal shift to the left in the second image.
 - C. A large right-sided pneumothorax with mediastinal shift to the left in both the first and second images.
 - D. A large left-sided pneumothorax with no mediastinal shift in the first image, and a large right-sided pneumothorax with mediastinal shift to the right in the second image.
 - E. A large left-sided pneumothorax with mediastinal shift to the left in the first image, and a large right-sided pneumothorax with mediastinal shift to the right in the second image.
 - F. A small right-sided pneumothorax with no mediastinal shift in the first image, and a large left-sided pneumothorax with mediastinal shift to the right in the second image.
-

Answer: A

Reason:

The first image shows a large left-sided pneumothorax, evidenced by the additional line between the third and fourth ribs and the collapse of the left lung, with mediastinal structures displaced to the right. The second image depicts a large right-sided pneumothorax, as indicated by the significant collapse of the right lung and mediastinal shift to the left. These findings are consistent with the descriptions provided in both images.

Figure 12: Two Frames Example

Example - #2

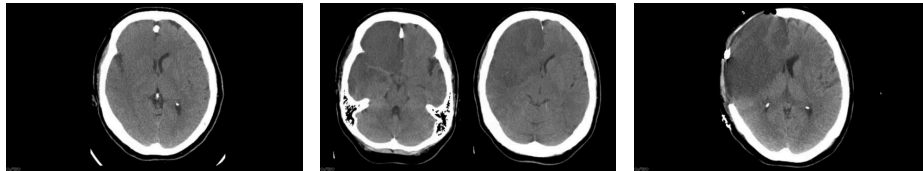
System: central nervous system

Organ: brain

Modality: CT

YouTube Link: <https://youtu.be/eoxKSAoGW2s>

.....
Input Images:



Question:

Based on the imaging findings across the first, second, and third images, which of the following best describes the most likely etiology and current stage of the observed pathology?

Options:

- A. Acute ischemic stroke involving the right anterior cerebral artery and middle cerebral artery territories with significant mass effect and early signs of herniation.
- B. Chronic ischemic changes in the right cerebral hemisphere with resolved mass effect and no evidence of acute intervention.
- C. Acute hemorrhagic stroke in the right cerebral hemisphere with associated midline shift and ventricular compression.
- D. Acute ischemic stroke involving the left anterior cerebral artery and middle cerebral artery territories with no significant mass effect.
- E. Subacute ischemic stroke in the right cerebral hemisphere with complete resolution of midline shift following surgical intervention.
- F. Acute ischemic stroke involving the right anterior cerebral artery and middle cerebral artery territories with persistent mass effect despite surgical decompression.

.....
Answer: A

Reason:

The correct answer is derived by integrating the following visual findings: (1) The first image shows diffuse parenchymal hypodensity, sulcal effacement, and poor gray-white differentiation in the right hemisphere, consistent with acute ischemic stroke. (2) The second image highlights a well-defined area of low attenuation involving the anterior and middle cerebral artery territories, with significant mass effect, ventricular compression, and midline shift, further supporting acute ischemic stroke with complications. (3) The third image confirms the persistence of poor gray-white differentiation and mass effect, despite surgical decompression, indicating an acute stage of ischemic stroke with ongoing complications. The other options are incorrect because they either misidentify the hemisphere, mischaracterize the pathology as hemorrhagic, or incorrectly describe the stage or resolution of the findings.

Figure 13: Three Frames Example

Example - #3

System: musculoskeletal system

Organ: spine

Modality: X-ray

YouTube Link: https://youtu.be/U57_gD8Ftkw

Input Images:



Question:

Based on the radiographic findings across the described images, which combination of features most strongly supports the diagnosis of advanced intervertebral disc degeneration at L4-5 compared to L5-S1?

Options:

- A. Significant disc narrowing at L4-5 to 3-4 mm, sclerosis of the end plates, and absence of a vacuum phenomenon.
- B. Disc narrowing at L4-5 to 3-4 mm, intact end plates without sclerosis, and whitening of the end plates due to prolonged stress.
- C. Disc narrowing at L4-5 to 3-4 mm, sclerosis of the end plates, whitening of the end plates, and absence of fluid leading to a vacuum phenomenon.
- D. Thick disc at L5-S1 measuring 12-13 mm, intact end plates without sclerosis, and absence of a vacuum phenomenon.
- E. Disc narrowing at L4-5 to 3-4 mm, intact end plates without sclerosis, and thick disc at L5-S1 measuring 12-13 mm.
- F. Disc narrowing at L4-5 to 3-4 mm, sclerosis of the end plates, whitening of the end plates, and thick disc at L5-S1 measuring 12-13 mm.

Answer: C

Reason:

The correct answer integrates multiple visual findings described across the images. The significant narrowing of the L4-5 disc space to 3-4 mm is a hallmark of advanced degeneration, as noted in all images. Sclerosis of the end plates at L4-5 is explicitly described in image_2 and image_3, indicating chronic stress. Whitening of the end plates due to prolonged stress is mentioned in image_3 and image_4, further supporting degeneration. The vacuum phenomenon, described in image_3 and image_4, is a key feature of advanced degeneration, where gas accumulates in the disc space due to fluid loss. These findings collectively point to advanced intervertebral disc degeneration at L4-5 compared to L5-S1, which remains thicker and less degenerated.

Figure 14: Four Frames Example

Example - #4

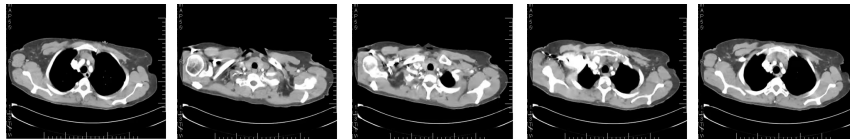
System: respiratory system

Organ: lung

Modality: CT

YouTube Link: <https://youtu.be/rmX9AeGYscU>

.....
Input Images:



Question:

In the provided CT angiography images of the chest, which anatomical structure is most likely to serve as the primary landmark for orienting the scan and differentiating between the mediastinal and pulmonary vasculature regions?

Options:

- A. Aortic arch
- B. Left atrium
- C. Right pulmonary artery
- D. Superior vena cava
- E. Descending thoracic aorta
- F. Main pulmonary artery

.....
Answer: A

Reason:

The aortic arch is explicitly described across all images as the key landmark for orientation in the CT angiography scans. It is a readily identifiable structure that helps in distinguishing the mediastinal anatomy from the pulmonary vasculature. Other options, such as the left atrium or right pulmonary artery, are part of the chest anatomy but are not emphasized as primary orientation landmarks in the described images.

Figure 15: Five Frames Example